

FAST REGULARIZED LINEAR SAMPLING
FOR INVERSE SCATTERING PROBLEMS
by M. Fares¹, S. Gratton² and Ph. L. Toint³
Report 09/08 19 March 2009

¹ CERFACS,
42, avenue Coriolis, 31057 Toulouse Cedex 01, France
email: fares@cerfacs.fr

² Centre National d'Etudes Spatiales (CNES),
18, avenue Edouard Belin, 31401 Toulouse, France
email: gratton@cerfacs.fr

¹ Department of Mathematics,
FUNDP-University of Namur,
61, rue de Bruxelles, B-5000 Namur, Belgium.
email: philippe.toint@fundp.ac.be

Fast regularized linear sampling for inverse scattering problems

M'Barek Fares, Serge Gratton and Philippe L. Toint

19 March 2009

Abstract

A new numerical procedure is proposed for the reconstruction of the shape and volume of unknown objects from measurements of their radiation in the far field. This procedure is a variant of the linear sampling method and has a very acceptable computational load and is fully automated. It is based on exploiting an iteratively computed truncated singular-value decomposition and heuristics to extract the desired signal from the background noise. Its performance on a battery of examples of different types is shown to be promising.

Keywords: inverse scattering, linear sampling method, regularization heuristics, numerical algorithms.

1 Introduction

The Linear Sampling Method (LSM) has recently been the object of a growing interest in inverse scattering problems (see Arens, 2004, Cakoni, Colton and Haddar, 2002, Cakoni and Colton, 2003, Colton, Haddar and Monk, 2002, Colton, Haddar and Piana, 2003, or Haddar and Monk, 2002, for instance). This interest is due to its effectiveness, especially in treating three-dimensional inverse problems, but also to its large spectrum of applications. We recall that this algorithm allows the reconstruction of the shape of an obstacle (or a local inhomogeneity) from multistatic data at a fixed frequency. Unlike classical nonlinear methods, it is based on solving independent linear systems and requires no a priori knowledge on the physical properties of the scatterers.

This paper follows the earlier contribution of Collino, Fares and Haddar (2003), who consider the numerical solution of the inverse LSM problem in electromagnetics. Their algorithm reduces the task to the solution of a collection of independent linear inverse problems corresponding to the available far-field measurements, which are independently regularized using the Tikhonov-Morosov discrepancy principle (Colton, Piana and Potthast, 1997). The final reconstruction involves manual tuning of level curves using a mathematical plotting tool. Specifically, the numerical solution is based on the singular-value decomposition of a dense matrix whose dimension is directly proportional to the number of vertices of the chosen discretization of the sphere on which far-field measurements are taken. The combination of these techniques has proved to be quite successful in the reconstruction of the shape of non-trivial objects from simulated observations. The reader is referred to Collino et al. (2003) for more details.

While possibly adequate in electromagnetics where the number of measurements remains manageable, difficulties arise when considering applications in acoustics such as medical echography, where the number of measurements is potentially much larger. This makes the singular-value decomposition impractical. Moreover, the final manual level-curve tuning can be considered as a drawback since it directly affects the estimation of the (*a priori* unknown) shape and volume of the reconstructed object, which is difficult in the absence of *a priori* information, and then results in interpretation uncertainties.

It is the purpose of the present paper to propose a technique avoiding those difficulties. We first introduce iterative methods to replace the full singular-value decomposition by a truncated one. We then describe a technique for replacing hand-tuned graphical plots by an automatic level surface selection whose advantage is to provide a good estimation of the actual size of the reconstructed object. Experiments will be presented on a collection of problems of different shapes and topological structures.

The paper is organized as follows. Section 2 describes the LSM technique for recovering objects from far-field measurements. Our algorithm and heuristics are then presented in Section 3, while numerical experiments are discussed in Section 4. Conclusions and perspectives are finally outlined in Section 5.

2 A brief description of the LSM

2.1 The forward problem

Suppose a bounded (sound-soft) domain $D \subset \mathbb{R}^3$ of class \mathcal{C}^2 is given. This domain is illuminated by a plane wave incident field $u^{\text{inc}}(x, d) = e^{ikx \cdot d}$, $x \in \mathbb{R}^3$, for some $d \in S$, where S is the unit sphere. The forward problem consist in finding a function $u^s \in \mathcal{C}^2(\mathbb{R}^3 \setminus \overline{D}) \cap \mathcal{C}(\mathbb{R}^3 \setminus D)$ that satisfies

$$\Delta u^s + k^2 u^s = 0 \quad \text{in } \mathbb{R}^3 \setminus \overline{D}, \quad (2.1)$$

$$u = u^{\text{inc}} + u^s, \quad (2.2)$$

$$u = 0 \quad \text{on } \partial D, \quad (2.3)$$

$$\lim_{r \rightarrow \infty} \left(\frac{\partial u^s}{\partial r} - iku^s \right) = 0, \quad (2.4)$$

where $k > 0$ is the wave number. The function u^s is called the scattered wave. In case of sound-hard obstacle, the boundary condition (2.3) is replaced by

$$\frac{\partial u}{\partial \nu} = 0 \quad \text{on } \partial D, \quad (2.5)$$

where ν is the normal to ∂D directed towards the exterior of D . The condition (2.4) characterizes outgoing waves and ensures uniqueness of the solution of the scattering problem. Any solution u^s to the forward problem (2.1) is called radiating. It can be shown (Colton and Kress, 1998) that every radiating solution u to the Helmholtz equation has the asymptotic behaviour of an outgoing spherical wave

$$u(x, d) = \frac{e^{ik\|x\|}}{\|x\|} \left\{ u^\infty(\hat{x}, d) + O\left(\frac{1}{\|x\|}\right) \right\}, \quad \|x\| \rightarrow \infty \quad (2.6)$$

uniformly in all directions $\hat{x} = x/\|x\|$, where u^∞ , defined on the unite sphere S is known as the far-field pattern of u and $\|x\|$ is the Euclidean norm of x .

2.2 The inverse problem and the LSM

We are interested in the inverse problem consisting of the reconstruction of the domain D from the knowledge of $u^\infty(\hat{x}, \hat{d})$ for all $(\hat{x}, \hat{d}) \in S \times S$ for a fixed, known wave number k . The far-field pattern $u^\infty(\hat{x}, \hat{d})$ defines the far-field operator $F : L^2(S) \rightarrow L^2(S)$ by

$$(Fg)(\hat{x}) = \int_S u^\infty(\hat{x}, d)g(d)ds(d). \quad (2.7)$$

The linear sampling method chooses a position $z \in \mathbb{R}^3$ and then looks for the solution $g = g(\cdot, z) \in L^2(S)$ of the far-field equation

$$(Fg)(\hat{x}) = \Phi_\infty(\hat{x}, z) = e^{-ik\hat{x}\cdot z}/4\pi \quad (2.8)$$

where $\Phi_\infty(\hat{x}, z)$ is the far-field pattern associated with plane wave $e^{ik\hat{x}\cdot z}$. Notice first that since F is compact, equation (2.8) is ill posed. Even if this equation does not have any solution in general (Colton, 2003), it turns out that one can prove the existence of a nearby solution $g_\varepsilon(\cdot, z) \in L^2(S)$, in the sense that it satisfies the inequality $\|Fg_\varepsilon(\cdot, z) - u^\infty(\cdot, z)\| \leq \varepsilon$, where ε is a small parameter independent of z , such that

$$\lim_{\substack{z \rightarrow \partial D \\ z \in D}} \|g_\varepsilon(\cdot, z)\|_{L^2(S)} = \infty. \quad (2.9)$$

Furthermore, (formally) $\|g_\varepsilon(\cdot, z)\| = \infty$ for $z \in \mathbb{R}^3 \setminus D$ (again, see Colton, 2003). Consequently the L^2 -norm of $g_\varepsilon(\cdot, z)$ can be used as an indicator of the domain D that we want to reconstruct. Broadly speaking, this is the main idea of the LSM.

2.3 Analytical expression of the far fields for a sphere

For illustrative purposes, we consider in this section the case where the scatterer is a sphere of a radius R .

The derivation of an analytic expression of the far-field $u^\infty(\cdot, d)$ relies on the decomposition of the incident and scattered fields (Colton and Kress, 1998, pp. 32 and 53, for instance), which can be written as

$$\begin{aligned} e^{ikx\cdot d} &= \sum_{n=0}^{\infty} i^n (2n+1) j_n(k|x|) P_n(\cos \theta) \\ &= \sum_{n=0}^{\infty} \sum_{m=-n}^n 4\pi i^n j_n(k|x|) \overline{Y_n^m(d)} Y_n^m(\hat{x}), \end{aligned} \quad (2.10)$$

and

$$u_\infty(\hat{x}, d) = \sum_{n=0}^{\infty} \sum_{m=-n}^n \frac{4i\pi}{k} \frac{j_n(kR)}{h_n^{(1)}(kR)} \overline{Y_n^m(d)} Y_n^m(\hat{x}) = \sum_{n=0}^{\infty} \sum_{m=-n}^n u_n \overline{Y_n^m(d)} Y_n^m(\hat{x}) \quad (2.11)$$

respectively, where (Y_n^m) denotes the set of orthonormal spherical harmonics, (j_n) denotes the set of spherical Bessel functions of the first kind, $(h_n^{(1)})$ denotes the set of spherical Hankel functions of the first kind, and P_n denotes the Legendre polynomials.

Looking for a solution $g_z(d)$ of the form

$$g_z(d) = \sum_{n=0}^{\infty} \sum_{m=-n}^n g_n^m(z) Y_n^m(d), \quad (2.12)$$

we find that

$$\int_S u_\infty(\hat{x}, d) g_z(d) ds(d) =$$

$$\begin{aligned}
 &= \int_S \left(\sum_{n=0}^{\infty} \sum_{m=-n}^n u_n \overline{Y_n^m(d)} Y_n^m(\hat{x}) \right) \left(\sum_{k=0}^{\infty} \sum_{m=-k}^k g_k^j(z) Y_k^j(d) \right) ds(d) \\
 &= \sum_{k=0}^{\infty} \sum_{n=0}^{\infty} \sum_{j=-k}^k \sum_{m=-n}^n u_n g_k^j(z) Y_n^m(\hat{x}) \int_S \overline{Y_n^m(d)} Y_k^j(d) ds(d) \\
 &= \sum_{n=0}^{\infty} \sum_{m=-n}^n u_n g_n^m(z) Y_n^m(\hat{x})
 \end{aligned}$$

Using (2.7), (2.8), (2.10) and this last expression, we deduce that

$$u_n g_n^m(z) = (-i)^n j_n(k||z||) \overline{Y_n^m(z)},$$

and thus that

$$g_n^m(z) = \frac{(-1)^n i^{n-1} k j_n(k||z||)}{4\pi j_n(kR)} h_n^{(1)}(kR) \overline{Y_n^m(z)}$$

Substituting this expression in (2.12), we finally obtain that

$$\begin{aligned}
 g_z(d) &= \sum_{n=0}^{\infty} \sum_{m=-n}^n \frac{(-1)^n i^{n-1} k j_n(k||z||)}{4\pi j_n(kR)} h_n^{(1)}(kR) \overline{Y_n^m(z)} Y_n^m(d) \\
 &= \sum_{n=0}^{\infty} \sum_{m=-n}^n v_n \overline{Y_n^m(z)} Y_n^m(d).
 \end{aligned}$$

Using the orthonormality of (Y_n^m) we have that

$$\|g_z\|^2 = \sum_{n=0}^{\infty} \sum_{m=-n}^n |v_n|^2 |Y_n^m(z)|^2 = \sum_{n=0}^{\infty} |v_n|^2 \sum_{m=-n}^n |Y_n^m(z)|^2 = \sum_{n=0}^{\infty} |v_n|^2 \frac{2n+1}{4\pi}.$$

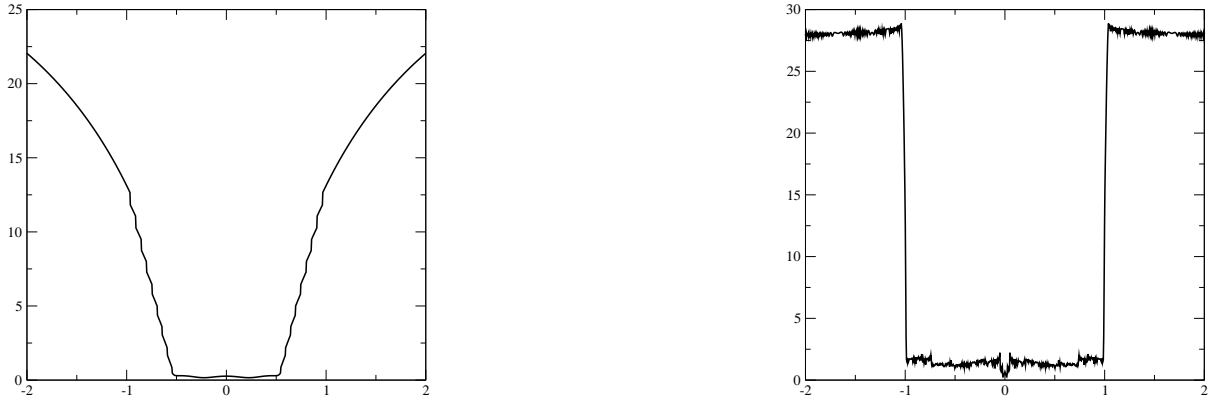
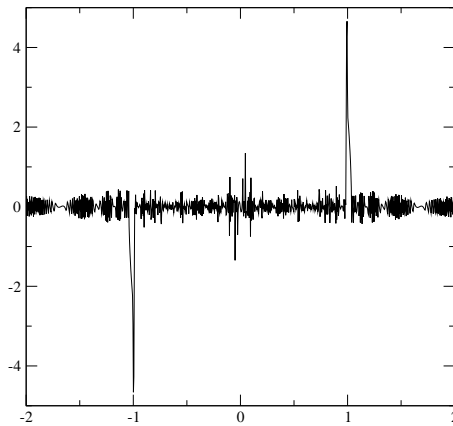
A simple calculation then yields

$$\|g_z\| = \sqrt{\sum_{n=0}^{\infty} \frac{(2n+1)k^2}{(4\pi)^2} \left\{ 1 + \left[\frac{y_n(kR)}{j_n(kR)} \right]^2 \right\} [j_n(k||z||)]^2},$$

where (y_n) are the spherical Bessel functions of the second kind. The function $\|g_z\|$ is pictured in Figure 1 (for z on a line passing through the center of the sphere) for wave numbers $k = 10$ and $k = 5000$, respectively. The gradient of $\|g_z\|^{-1}$ for $k = 5000$ is also shown in Figure 2. As expected, the boundary of the sphere closely coincides with well-defined peaks in the magnitude of this gradient, an observation which we exploit below.

3 Numerical algorithms

Having described the continuous problem and shown some of its features on a simple example, we now consider the practical numerical computation of its solution.


 Figure 1: Values of $\log_{10} \|g_z\|$ for $k = 10$ (left) and $k = 5000$ (right)

 Figure 2: Values of the gradient ($\log_{10} \|\nabla_z g_z\|$) for $k = 5000$

3.1 The continuous Morozov regularization

We start by recalling the technique used by Collino et al. (2003). We adopt here the same discretization scheme of the far-field equation (2.8) as the one used in Colton, Giebermann and Monk (2000). We consider a triangular mesh of the unit sphere S containing N vertices $(d_i)_{1 \leq i \leq N}$. These vertices serve as directions for the plane incident waves as well as degrees of freedom for the discrete solution of the far-field equation. As an empirical rule we take $N \simeq (kR + 2 \log(kR + \pi))^2$ where R is the radius of a sphere containing the object. This rule can be inferred by studying the spectrum of the far field as functions of the object size.

For the numerical realization of the LSM, we construct a continuous approximation of the solution $g(\cdot, z)$ linear at each triangle, whose degrees of freedom are its values at the nodes $(d_i)_{1 \leq i \leq N}$. The nodal values are denoted by $(g_j(z))_{1 \leq j \leq N}$.

We assume that an approximate far-field pattern $F_{i,j}^\infty \simeq u^\infty(d_i, d_j)$, $i, j = 1, \dots, N$ is known for N incident plane wave with directions d_i and measured in the same directions.

The integral equation (2.8) can be transformed at the discrete level into the following linear system of N unknowns (g_j):

$$\sum_{j=1}^N \omega_j F_{q,j} g_j = e^{-ikz d_q \cdot z}, \quad q = 1, \dots, N, \quad (3.13)$$

where the weights ω_j are linked to the quadrature formulae used in evaluating the integrals over the mesh triangles.

For each z , the system (3.13) is then a discretized $N \times N$ linear system of the form

$$Fg(z) = b^\infty(z) \stackrel{\text{def}}{=} \left(e^{-ikd_1 \cdot z}, \dots, e^{-ikz d_N \cdot z} \right)^T \quad (3.14)$$

where F is $N \times N$ matrix independent of z , $g(z) = (g_1(z), \dots, g_N(z))^T$ is the unknown vector whose ℓ_2 norm is expected to be large when z is outside D and finally $b^\infty(z)$ is the right-hand side constructed from the far field of the plane waves $u^{\text{inc}}(z, d_j)$ for $j = 1, \dots, N$. Because this system is ill-defined, a Tikhonov regularization is used for the solution of (3.14), namely by seeking $g_\eta(z)$ solution of

$$(F^*F + \eta(z)I)g_\eta(z) = F^*b^\infty(z) \quad (3.15)$$

where $\eta(z)$ is a regularization parameter depending on z which is determined using the Morozov discrepancy principle (Colton et al., 1997). More specifically, $\eta(z)$ is chosen as the root of the discrepancy function

$$\|Fg_\eta(z) - b^\infty(z)\|^2 - \delta^2 \|g_\eta(z)\|^2 \quad (3.16)$$

where δ is an estimate of the error on the matrix F .

For practical purposes, a box \mathcal{B} of \mathbb{R}^3 containing the object (more or less at its centre) is discretized using a regular cubic mesh and we denote by \mathcal{Z} the set of all these discretized points. The system (3.14) is then solved for each $z \in \mathcal{B}$, using the singular-value (SVD) decomposition of the matrix F given by

$$F = U\Sigma V^* \quad (3.17)$$

where U and V are unitary and Σ is real diagonal with $\Sigma_{i,i} = \sigma_i$, $1 \leq i \leq N$.

Once the set of solutions $\{g_\eta(z)\}_{z \in \mathcal{B}}$ is known from

$$g_\eta(z) = V [\Sigma + \eta(z)I]^{-1} U^* b^\infty(z),$$

a graphical tool (Gnuplot) is used to plot the level surfaces of the function $\|g_\eta(z)\|^{-1}$, and the ‘‘most likely’’ such surface is finally selected by trial and error, hopefully representing the unknown object.

As indicated above, this procedure produces excellent results in the sense that the reconstructed object are visually very sharp (see Section 4). However, it suffers from the high cost of the full singular-value decomposition (3.17), which makes it essentially inapplicable to large-scale problems. The adhoc nature of the final graphical tuning is a serious drawback if the procedure is to be automated as part of a more complicated application.

3.2 A truncated singular-value decomposition

The new approach considers computing the SVD (3.17) incrementally by using a subspace iteration, possibly stopping the calculation at a (very) early stage if the desired accuracy is obtained. Using truncated SVD for this purpose is not a new idea: we refer the reader to Hansen (1997) for further description and analysis of this approach, often called the truncated SVD regularization. This

technique has the advantage that it does not require the full decomposition of a (potentially large) dense matrix, in contrast with the Tikhonov-Morosov approach. It is also particularly well suited to the case where many right-hand sides are considered, which is our case since we need a solution of (3.14) for each $z \in \mathcal{B}$.

Assume first that we know an integer $1 \leq p \leq N$ such that the unknown object can be well represented by the contribution of the p left singular vectors corresponding to the largest singular values. Then a truncated SVD (TSVD) approach (see Hansen, 1997) can be used. In such an approach, one needs to compute U_p , the matrix whose columns are the p considered left singular vectors. More specifically, we proceed by first selecting a block size $1 \leq \tau \leq N$ and perform the subspace iterations (see Chapter 6 in Stewart, 1998), given by

$$W_{k+1} = FF^*U_k, \quad W_{k+1} = U_{k+1}R_{k+1}$$

where the last step is the usual QR factorization. The iteration is initialized with a random $\tau \times n$ matrix V_0 and terminated as soon as

$$\|FF^*U_k - U_k(U_k^*FF^*U_k)\|_F \leq \epsilon\sqrt{\tau}\|F\|_F$$

where $\|\cdot\|_F$ is the Frobenius norm and ϵ is a convergence tolerance (10^{-5} in our tests). At convergence, the columns of U_k (approximately) span the left invariant subspace corresponding to the τ largest singular values of A . If a larger invariant subspace is needed, that is if less than p largest singular values and associated left singular vectors have been computed so far, the iteration is restarted with the matrix F replaced by the deflated matrix $(I - U_c U_c^*)F$, where the columns of U_c are the previously computed singular vectors. This then gives the next τ largest singular values and associated left singular vectors. The process is repeated ℓ times, where ℓ is the smallest integer such that $p \leq \ell\tau$, and the matrices U_p and Σ_p are constructed.

We may then approximate the solution of (3.14) by

$$g_p(z) = U_p(U_p^*FF^*U_p)^{-1}U_p^*b^\infty(z) \quad (3.18)$$

and define

$$\psi_p(z) \stackrel{\text{def}}{=} \|g_p(z)\|^{-1} = \|(U_p^*FF^*U_p)^{-1}U_p^*b^\infty(z)\|^{-1} = \|\Sigma_p^{-1}U_p^*b^\infty(z)\|^{-1}$$

The performance of this algorithm relies on the choice of a suitable number $p_\diamond(z)$ of singular vectors used to represent the solution of (3.14), that is a number such that the signal contained in $\{\psi_{p_\diamond(z)}(z)\}_{z \in \mathcal{B}}$ clearly emerges from noise and is not yet contaminated by too much high frequency.

3.3 An L-curve approximation of the Morozov principle

We now describe a technique for computing $p_\diamond(z)$, based on the notion of ‘‘L-curve’’ (see Hansen, 1997). At each z , we define the discrete L-curve given by $\|g_p(z)\|$ as a function of $\|Fg_p(z) - b^\infty(z)\|$. Such a curve starts (for large p) with high values of the solution norm and decreases with p until the solution norm is small and the residual norm large.

For a given z , we then consider all values of $p = 1, 2, \dots$ until we find the first value $p(z)$ such that

$$\|Fg_p(z) - b^\infty(z)\| \leq \delta\|g_p(z)\|. \quad (3.19)$$

Since this inequality is violated for $p = 1$ because the residual is then too large, the value $p(z)$ defines a discrete approximation of the root (3.16).

3.4 Reconstructing the object

Our example of the radiating sphere suggests that the boundary of the object is characterized by large values of the gradient of $\psi_{p(z)}$. Our proposal is based on this observation and uses the segment \mathcal{S} , which we define as the (discretized) main diagonal of the box \mathcal{B} . We then restrict the function $\psi_{p(z)}$

$$c(z) = \psi_{p(z)}(z) \quad \text{for } z \in \mathcal{S},$$

and determine the level of $\psi_{p(z)}$ corresponding to large gradients on this segment. In practice, we determine the position $z_\diamond \in \mathcal{S}$ such that the derivative of $c(z)$ is maximum in absolute value, i.e.

$$z_\diamond = \arg \max_{z \in \mathcal{S}} \left| \frac{dc}{dz}(z) \right|,$$

where the derivative is approximated by finite differences. The boundary of the unknown object is finally reconstructed as the level surface \mathcal{L}_\diamond defined by

$$\mathcal{L}_\diamond \stackrel{\text{def}}{=} \{z \in \mathcal{B} \mid \psi_{p(z)}(z) = \frac{1}{2}c(z_\diamond)\}, \quad (3.20)$$

where the factor $\frac{1}{2}$ was found best in our experiments. We emphasize that the heuristic described in this section can be considered as a reasonable starting point for further “manual” tuning.

4 Numerical experiments

We now present numerical experiments with our method on a battery of five examples in the acoustic domain: a cross, a teapot, a rocket, a plane and a Σ shaped object. For each of these examples, we discretized the sphere in 2252 directions and discretized \mathcal{B} using $50 \times 50 \times 50$ points. Other parameters for these examples are given in Table 1.

example	k	$[\underline{x}, \bar{x}]$	$[\underline{y}, \bar{y}]$	$[\underline{z}, \bar{z}]$	$[\underline{X}, \bar{X}]$	$[\underline{Y}, \bar{Y}]$	$[\underline{Z}, \bar{Z}]$
cross	10	$[-0.625, 0.625]$	$[-0.625, 0.625]$	$[-0.125, 0.125]$	$[-1, 1]$	$[-1, 1]$	$[-0.5, 0.5]$
teapot	31	$[-0.3, 0.34]$	$[-0.2, 0.2]$	$[0, 0.315]$	$[-0.5, 0.5]$	$[-0.5, 0.5]$	$[-0.1, 0.4]$
rocket	20	$[-0.165, 0]$	$[-0.241, 0.241]$	$[-0.241, 0.241]$	$[-2, 0.5]$	$[-0.5, 0.5]$	$[-0.5, 0.5]$
plane	12	$[-0.101, 0.101]$	$[-0.129, 0.75]$	$[-0.188, 0.416]$	$[-1.3, 1.3]$	$[-1.6, 1]$	$[-0.5, 0.5]$
Σ	30	$[-1, 0.8]$	$[-0.9, 0.9]$	$[-0.5, 0]$	$[-1.3, 1.1]$	$[-1.2, 1; 2]$	$[-0.8, 0.3]$

Table 1: Geometric parameters for the tested examples

In this table, k is the wave number of the incident wave, $[\underline{x}, \bar{x}]$, $[\underline{y}, \bar{y}]$, and $[\underline{z}, \bar{z}]$ are the intervals (in x , y and z) defining the smallest box containing the object, and $[\underline{X}, \bar{X}]$, $[\underline{Y}, \bar{Y}]$ and $[\underline{Z}, \bar{Z}]$ are the intervals defining the scanned domain. The objects themselves are pictured on the top in Figures 3 to 7.

Our measurement matrix F was synthesized using CASC, a solver for acoustic scattering problems developed at CERFACS. In this package, the sound-soft case is treated by solving the integral equation,

$$S\varphi(x) = \int_{\partial D} \Phi(x, y)\varphi(y)ds(y) \quad x \in \partial D$$

whose unknown is $\varphi := [\partial_n \varphi] := \partial_n \varphi^+ - \partial_n \varphi^-$ and where $\Phi(x, y)$ is the fundamental solution to the Helmholtz equation. The numerical procedure is based upon a triangular meshing of the surface

and uses finite elements of lowest degree. It leads to solving for φ_h such that,

$$\begin{cases} \int_{\partial D_h} \int_{\partial D_h} \Phi(x, y) (\varphi_h(y) \cdot \varphi_h^{test}(x)) ds(y) ds(x) = - \int_{\partial D_h} u^{inc}(x) \varphi_h^{test}(x) ds(x), \\ \text{for all } \varphi_h^{test}(x) \end{cases}$$

The numerical computation amounts to solving a set of linear systems with a dense symmetric non-hermitian matrix whose size is the number of nodes of the mesh. There are as many right-hand sides as the number of incident directions. Special attention has been paid to properly taking into account the singularity of the Green kernel during the assembly process. The LU decomposition of the matrix is then performed by means of a set of ScaLAPACK parallel routines. Once φ_h has been obtained, the associated far fields are easily deduced by applying the integral representation formulae

$$u(x) = u^{inc}(x) + S\varphi(x) \quad x \notin \partial D.$$

For improved accuracy, care is taken to ensure that the length of the longest edge in the discretization does not exceed a tenth of the wavelength. Once the matrix F was generated, it was then perturbed by random noise of relative magnitude 0.01.

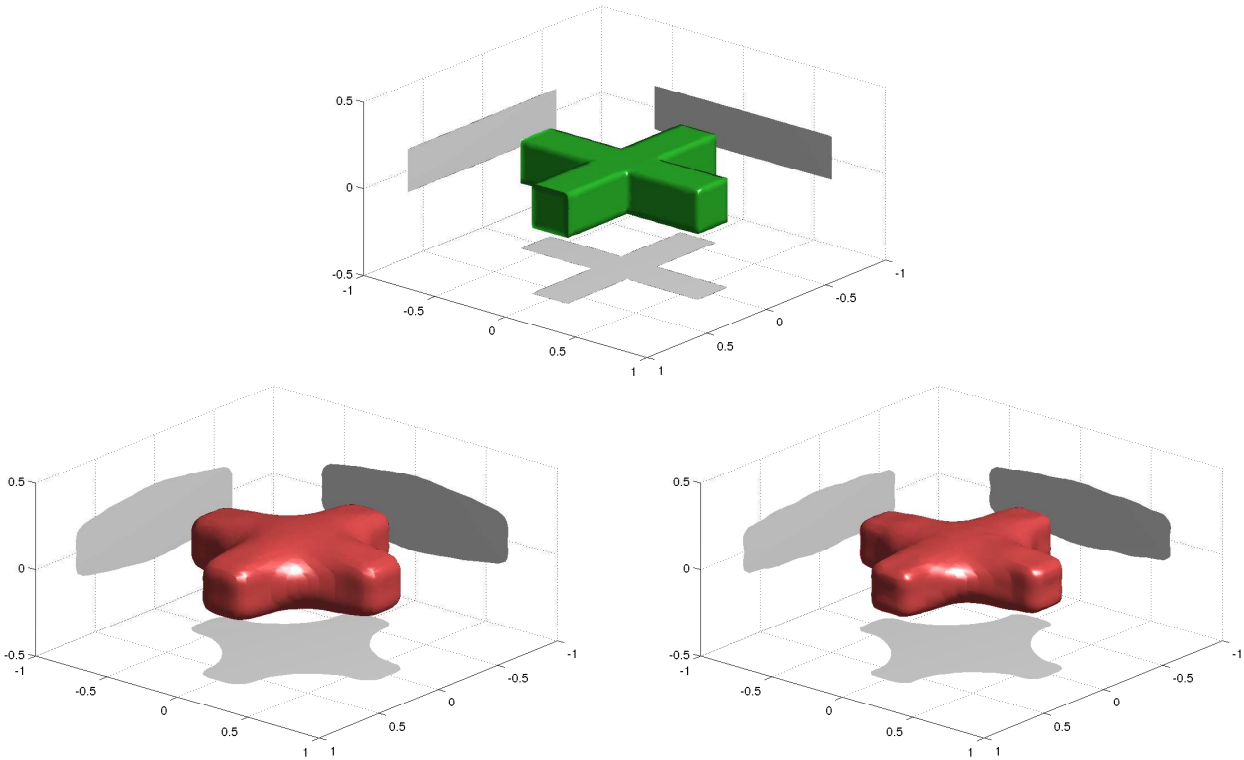


Figure 3: The cross: real (top) and reconstructed by Algorithms CTM (bottom left) and DTM (bottom right)

In Figures 3 to 7, we also show the reconstructed objects using two different algorithms.

1. The first of these algorithms is the method by Collino *et al.* described in Section 3.1, which uses the full singular-value decomposition (3.17), the continuous Tikhonov-Morosov regularization (3.15) depending on z . In what follows, we denote this method by the acronym CTM.

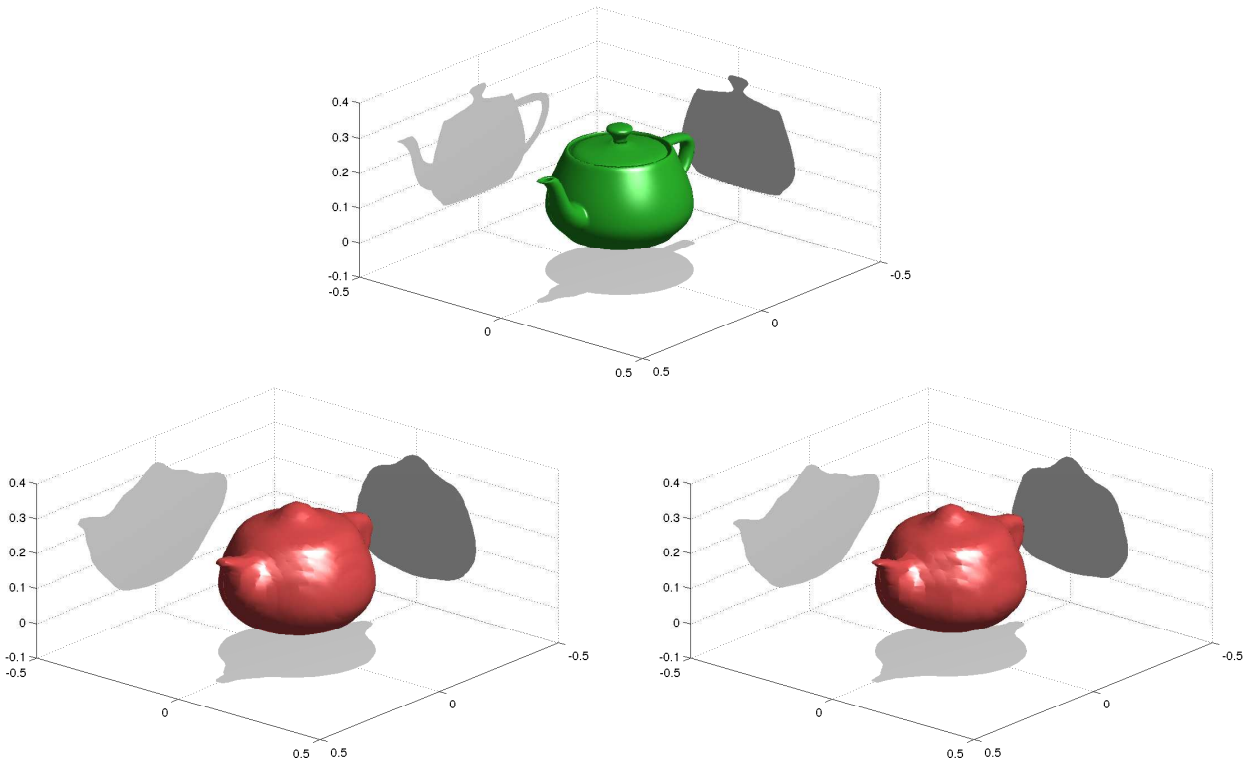


Figure 4: The teapot: real (top) and reconstructed by Algorithms CTM (bottom left) and DTM (bottom right)

2. The second algorithm, denoted DTM, uses the discrete Tikhonov-Morozov regularization described in Section 3.3. Although they result in the same image, two different computational variants may be considered:

- The first (DTM-F) computes the full SVD (3.17) and then selects the local regularization according to the strategy described in Section 3.3;
- the second (DTM-A) is more adaptive and only computes the necessary singular vectors by blocks¹ of size $\tau = 150$, using the subspace iteration of Section 3.2.

Examination of Figures 3 to 7 clearly shows that the “steepest slope” heuristic of Section 3.4 works reasonably well with methods CTM and DTM, and that the end-results produced by the two methods are very comparable. However, their computational requirements vary substantially, as we now discuss. To obtain a better idea of the relative weight of the main steps of the methods, we separated the computational time in three tasks:

1. the time required for computing the necessary left singular vectors and associated singular values
2. the time required for evaluating $\psi(z)$ for all $z \in \mathcal{B}$,
3. the time required to find the isovalue $c(z_\diamond)$

¹A single block turned out to be sufficient in all cases.

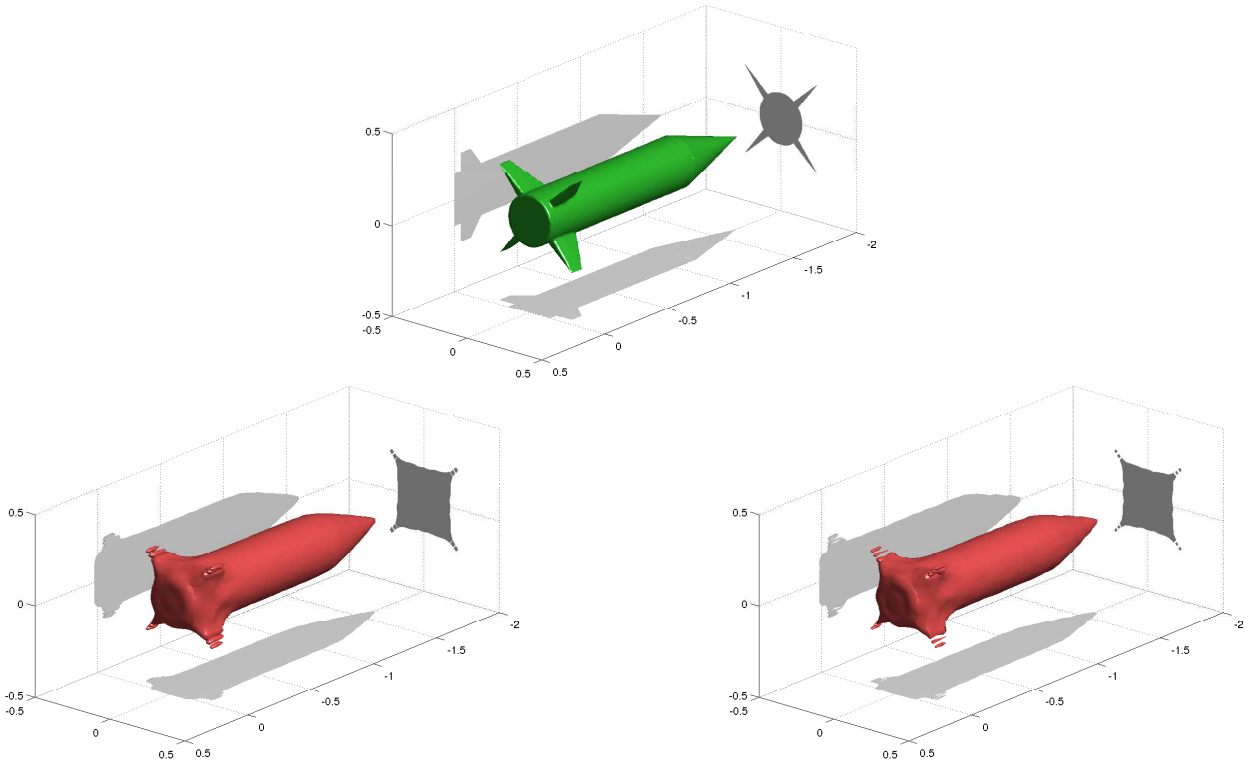


Figure 5: The rocket: real (top) and reconstructed by Algorithms CTM (bottom left) and DTM (bottom right)

The corresponding timings are given in Tables 2-4, for a Fortran 90 implementation of Algorithms CTM, DTM and TSVD, and were obtained on a single 1.6 GHz Itanium 2 processor of a Bull Novascale 3045 machine, using the MKL 64 library for linear algebra kernels. For comparison, we also included the computational times² for a third method (TSVD) where a global value³ of p_\diamond is used for all $z \in \mathcal{B}$.

	cross				teapot			
	CTM	DTM-F	DTM-A	TSVD	CTM	DTM-F	DTM-A	TSVD
SVD	1138.61	1138.61	43.99	43.99	1094.29	1094.29	47.30	47.30
eval. ψ	2083.44	80.66	100.06	130.92	1986.09	80.28	92.60	128.43
isovalue	16.84	0.63	0.79	-	15.91	0.63	0.73	-
total	3138.89	1219.90	144.84	-	3096.29	1175.2	140.53	-
percent.	100.00%	38.9%	4.6%	-	100.00%	37.9%	4.5 %	-

Table 2: CPU times (in secs.) for the different computational tasks and the four algorithms, applied on the cross and the teapot

As can be seen from these tables, Algorithm DTM-A is often twenty times faster than CTM, while DTM-F is merely approximately 2.5 times as fast. The only exception is the Σ problem, where convergence of the subspace iteration is slow in DTM-A, resulting in DTM-A being only

²We do not present the associated pictures because of space considerations and also because the determination of the level surface \mathcal{L}_\diamond is difficult to automate for this method.

³150 in our tests, a value which we knew was just slightly larger than strictly necessary.

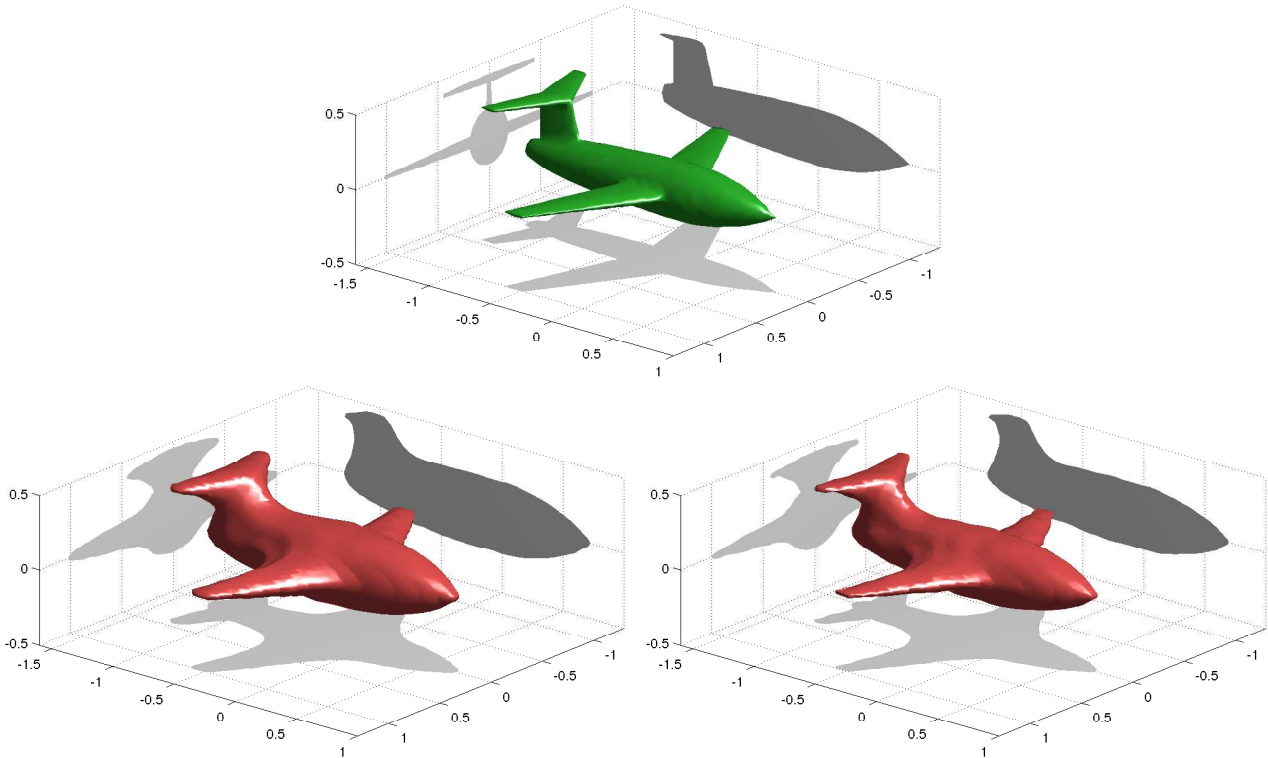


Figure 6: The plane: real (top) and reconstructed by Algorithms CTM (middle left) and DTM (bottom right)

about ten times faster than CTM.

5 Conclusion and perspectives

We have considered the use of the Linear Sampling Method for the solution of inverse scattering problems and have proposed a variant of the continuous Tikhonov-Morozov regularization which uses an adaptive technique for computing a suitable truncation level in the singular-value decomposition of the measurement's matrix. This adaptive technique makes use of subspace iteration to optimize computational costs. We have also considered a simple heuristic procedure for computing an isovalue of the solution which is suitable for an initial graphical representation.

The new variant is shown to be considerably more efficient than the original Tikhonov-Morozov

	rocket				plane			
	CTM	DTM-F	DTM-A	TSVD	CTM	DTM-F	DTM-A	TSVD
SVD	1092.77	1092.77	48.39	48.39	1147.75	1147.75	44.30	44.30
eval. ψ	1970.75	94.49	80.07	128.06	1950.52	95.45	103.08	127.36
isovalue	15.63	0.74	0.63	-	15.57	0.74	0.79	-
total	3079.15	1188.00	129.09	-	3113.84	1243.94	148.17	-
percent.	100.00%	38.6%	4.2%	-	100.00%	39.9%	4.8%	-

Table 3: CPU times (in secs.) for the different computational tasks and the four algorithms, applied on the rocket and the plane.

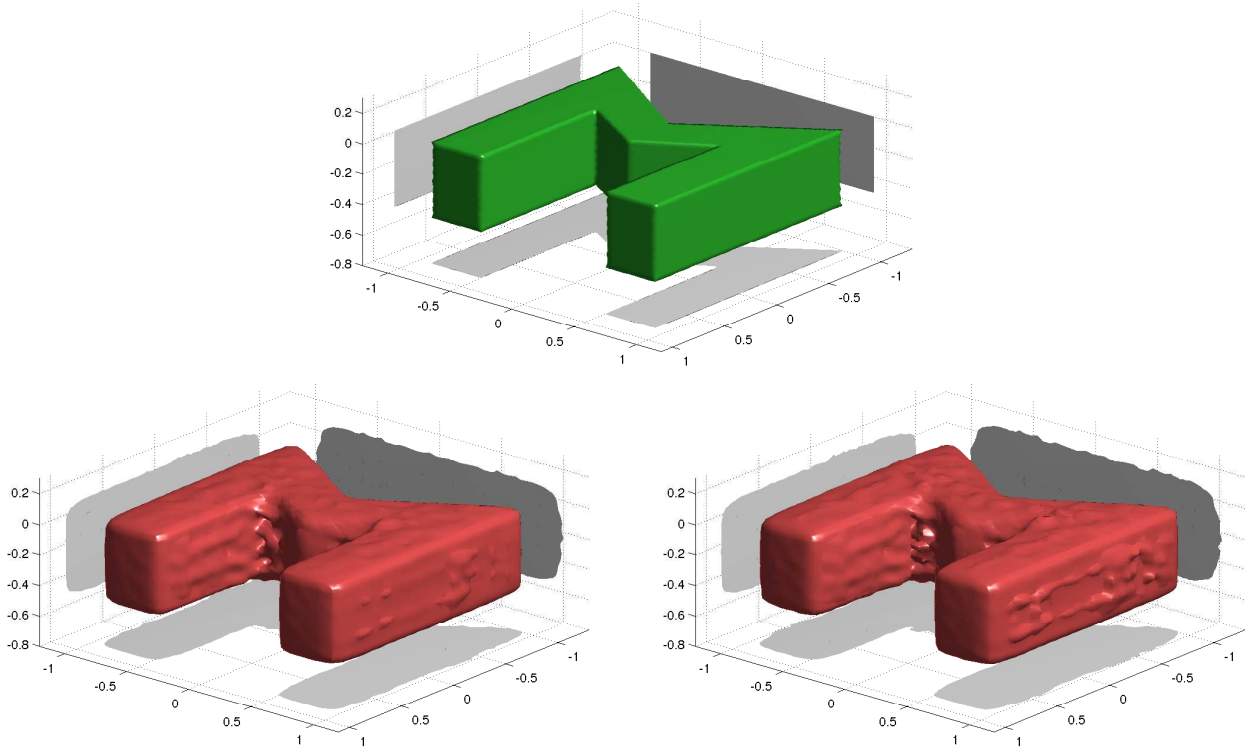


Figure 7: The Σ : real (top) and reconstructed by Algorithms CTM (bottom left) and DTM (bottom right)

technique, although the local nature of the regularization used still results in costs that may be avoided if the same regularisation parameter could be used for all points in the regularized domain. Further exploration of the potential of the truncated SVD is desirable in order to achieve this objective.

Acknowledgments

The authors would like to thank the C.I.C.T. (Centre Interuniversitaire de Calcul de Toulouse) for providing access to the Grid'MIP machine for producing the synthetic data.

	Σ			
	CTM	DTM-F	DTM-A	TSVD
SVD	1033.19	1033.19	241.95	241.95
eval. ψ	1944.66	80.77	92.00	127.54
isovalue	15.52	0.63	0.72	-
total	2993.37	1114.59	334.67	-
percent.	100.00%	37.2%	11.2%	-

Table 4: CPU times (in secs.) for the different computational tasks and the four algorithms, applied on the Sigma.

References

- T. Arens. Why linear the sampling method works. *Inverse Problems*, **20**, 163–173, 2004.
- F. Cakoni and D. Colton. A uniqueness theorem for an inverse electromagnetic scattering problem in inhomogeneous anisotropic media. *Proc. Edinburgh Math. Soc.*, **46**, 293–314, 2003.
- F. Cakoni, D. Colton, and H. Haddar. The linear sampling method for anisotropic media. *J. Comput. Appl. Math.*, **146**, 285–299, 2002.
- F. Collino, M. Fares, and H. Haddar. Numerical and analytical studies of the linear sampling method in electromagnetic scattering problems. *Inverse Problems*, **19**, 1279–1298, 2003.
- D. Colton. Inverse acoustic and electromagnetic scattering theory. *Inverse Problems*, **47**, 67–109, 2003.
- D. Colton and R. Kress. *Inverse Acoustic and Electromagnetic Scattering Theory*. Springer Verlag, 2nd edn, 1998.
- D. Colton, K. Giebermann, and P. Monk. A regularized sampling method for solving three-dimensional inverse scattering problems. *Sci. Comput.*, **21**(6), 2316–2330, 2000.
- D. Colton, H. Haddar, and P. Monk. The linear sampling method for solving the electromagnetic inverse scattering problem. *SIAM Journal on Scientific Computing*, **24**, 719–731, 2002.
- D. Colton, H. Haddar, and M. Piana. The linear sampling method in inverse electromagnetic scattering theory. *Inverse problems*, **19**, S105–S137, 2003.
- D. Colton, M. Piana, and R. Potthast. A simple method using Morozov's discrepancy principle for solving inverse scattering problems. *Inverse Problems*, **13**, 1477–1493, 1997.
- H. Haddar and P. Monk. The linear sampling method for solving the electromagnetic inverse medium problem. *Inverse Problems*, **18**, 891–906, 2002.
- P. C. Hansen. *Rank-Deficient and Discrete Ill-Posed Problems: Numerical Aspects of Linear Inversion*. SIAM, Philadelphia, USA, 1997.
- G. W. Stewart. *Matrix Computations: Basic Decompositions*. SIAM, Philadelphia, USA, 1998.